Open Access

Iraqi Journal of Industrial Research (IJOIR)

Journal homepage: http://ijoir.gov.iq

Photocatalytic Degradation of Acid Black 210 dye Using Fixed Bed Reactor Containing Zinc Oxide Nanoparticles: Effects and Box–Behnken Optimization

[1]Zahraa A. Najm*, [1]Mohammed A. Atiya, [2]Ahmed K. Hassan

[1]Department of Biochemical Engineering, Al-Khwarizmi College of Engineering, University of Baghdad, Iraq

[2]Research and Technology Center of Environment, Water and Renewable Energy, Scientific Research Commission, Ministry of Higher Education and Scientific Research, Iraq

Article information

Article history:
Received: October, 08, 2024
Accepted: January, 18, 2025
Available online: June, 14, 2025

Keywords:
Photocatalytic,
Fixed-bed column,
Zinc oxide nanoparticles,
Green method

Corresponding Author:
Zahraa A. Najm
zhraqylnjm@gmail.com

DOI:
https://doi.org/10.53523/ijoirVol12I1ID529

Abstract

The present study uses a continuous photo-catalytic approach to treat textile wastewater with Acid Black 210 (AB210). In an extract from eucalyptus leaves, zinc oxide nanoparticles (ZnO-NPs) were created using a liquid-phase reduction technique and utilized as heterogeneous catalysts. SEM, EDAX, and FTIR procedures were among the characterization methods used on (NPs). The produced NPs had a specific surface area of 26 m^2 /g and were discovered to be spherical and porous. The effect of the main parameters on the Photo-Catalytic degradation of AB210 was investigated through a continuous fixed-bed system. A photoreactor was used to investigate and analyze the variables affecting the continuous system the dye concentration (5–40 mg/L), the pollutant flow rate through the column (AB210 flow rate) (1–5 mL/min), the height of the catalyst inside the column (ZnO-NPs height) (0.5–1.5 cm), and the UV-intensity (6–24 W/m^2). The optimized parameters for the fixed-bed system were with a removal efficiency of 69% determined as 2.25 mL/min, 1.21 cm, 30 mg/L, and 15 W/m^2 for flow rate, ZnO-NPs height, AB210 concentration, and UV intensity respectively. This study demonstrates the potential of ZnO-NPs synthesized from green sources as effective catalysts in the treatment of dye-contaminated textile wastewater using a continuous photo-catalytic system.

1. Introduction

Water management is one of the most pressing issues confronting the world, particularly in light of the rising population and burgeoning industries [1]. Water pollution from various substances such as dyes has caused environmental and health issues. In general, diverse textile manufacturing operations contribute to releasing one-fifth of the world's dye production into water sources, resulting in detrimental consequences on human health and the aquatic ecology [2, 3]. Various treatment techniques, such as coagulation, flocculation, membrane treatment, ion exchange, and biological techniques, are used to remove dyes from contaminated water. However, it is well known that these dyes are extremely persistent and difficult to eliminate using standard treatment techniques [4, 5]. Research has been used to create effective strategies for eliminating these colors. Due to its high efficacy,

simplicity of use, and ease of operation, adsorption has been extensively used to treat wastewater containing dye contaminants [6, 7]. Additionally, advanced oxidation processes, which cause the production of (•OH), are considered promising [8, 9].

One of the important Advanced Oxidation Processes (AOPs), the photocatalytic process, uses semiconductors like TiO_2 [10] ZnS [11], ZnO [12], MgO, Co_3O_4 [13] and CuO [14] to produce •OH and other reactive oxidizing species. AOPs can eliminate both organic and inorganic pollutants [15, 16] AOPs are superior to conventional treatment methods because they don't have a problem with secondary waste material production or removal [17], [18]. There are currently methods, such as adsorption, that either concentrate or move the dye molecules in effluent into a diffuse phase [19, 20]. The photocatalytic technique is very important for dye degradation, CO_2 reduction, H_2 production, and sterilization [21, 22]. The specifications of zinc oxide photocatalyst qualify it to be used effectively in the remediation process. It features wide UV radiation absorption, a large abundance, chemical stability under UV radiation, and is non-toxic [23, 24]. The summary of the interaction process is given as follows: When light hits the surface of ZnO, charged electrons from the VB move into the (eCB-). Redox reaction occurs on the photo-excited ZnO surface, and •OH is produced as a result of valence band holes (hVB+) oxidizing water molecules and hydroxide ions The reactions below summarize the •OH production from ZnO NPs [25].

$$\text{Photocatalyst} + hv \rightarrow h_{VB}^{+} + e_{CB}^{-} \quad (1)$$

$$h_{VB}^{+} + e_{CB}^{-} \rightarrow \text{energy} \quad (2)$$

$$H_2O + h_{VB}^{+} \rightarrow {}^{*}OH + H^{+} \quad (3)$$

$$O_2 + e^{-} \rightarrow O_2{}^{*-} \quad (4)$$

$${}^{*}OH + \text{Dye} \rightarrow \rightarrow H_2O + CO_2 \quad (5)$$

$$O_2{}^{*-} + \text{Dye} \rightarrow \rightarrow H_2O + CO_2 \quad (6)$$

Metal oxide nanoparticles (including ZnO NPs) were created utilizing a variety of physical and chemical techniques such as milling, the sol-gel method, chemical vapor deposition, and many more [26, 27]. Nevertheless, the implementation of physio-chemical methods presents additional challenges, including concerns regarding toxicity, adverse environmental impacts, and the considerable costs associated with the necessary equipment [28, 29]. To address these limitations, a viable alternative lies in the adoption of a biological approach utilizing organisms such as algae, fungi, bacteria, or plants, which offers the potential for producing non-toxic and cost-effective nanoparticles applicable in diverse fields like food, cosmetics, medicine, and wastewater treatment [30, 31]. Plant extracts are rich in protein and phytochemical materials like sitosterol, luteolin, glycosides, flavonoids, and dexamethasone, which are considered reducing agents and stabilizers that have been successfully applied in research to produce ZnO NPs [32]. A variety of plants, including Caccinia macranthera [15], Passiflora caerulea fresh [33], peels of Passiflora foetida [34], Portulaca oleracea [35], Tridax procumbens Linn [36], Tephrosia purpurea [32], and Hibiscus rose [13] have used aqueous extracts of the (Tephrosia purpurea) plant to prepare ZnO NPs and examine the photocatalytic activity of these semiconductor nanoparticles to degrade methylene blue under sunlight.

Purpose of this research is to investigate a continuous photocatalytic system as a sustainable method of treating textile effluent that contains Acid Black 210 (AB210). Eucalyptus leaf extract was used to create zinc oxide nanoparticles (ZnO-NPs), which were then used as environmentally friendly catalysts. A 69% dye removal efficiency was attained by optimizing key operational parameters.

2. Experimental Work

2.1. Chemicals

In this study, each of the chemical compounds used was of high purity (99.9%). The eucalyptus globulus leaves used were picked up from the garden of Baghdad University, Iraq. The dye acid black 210 (AB210) was taken from the leather tanning factory (Karadaa Region) as shown in Table (1), chemical and physical properties of dye (AB210). $ZnSO_4$ was obtained from a central drug house (CDH) in India, while 100% ethanol was obtained from (CARLO ERBA) Reagents Company in France.

Table (1): Chemical and physical properties of acid black 210 (AB210) [32].

Molecular Formula	$C_{34}H_{25}K_2N_{11}O_{11}S_3$
Melting point	300 ℃
Solubility	Soluble in water
Types of dye	Tri-Azo dye (N═N)
Chemical Structure	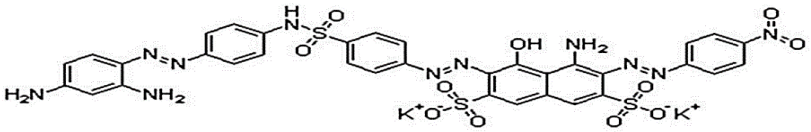

2.1.1. Leaf Extract Preparation

The synthesis process was adapted from [16] with minor changes. Initially, adopted the eucalyptus and cleaned it with distilled water to remove dust and tough dirt. The leaves were then oven-dried at 50 °C. When the leaves were sufficiently dry and crushable. The extract was prepared by using 10 g of powdered eucalyptus leaves and 150 mL of distilled water. The eucalyptus leaves and water was heated for 30 min at 80 ℃ by using a magnetic stirrer. The filtrate was then kept at 4 ℃ until it was used in zinc oxide nanoparticle preparation.

2.1.2. Photocatalyst Preparation

To prepare the ZnO-NPs, 1.61 g of solid $ZnSO_4$ was mixed with 100 mL of distilled water and stirred vigorously for 10 min. To remove contaminants, the solution was filtered using a 0.45 µm syringe filter. The eucalyptus extract was added gradually to the $ZnSO_4$ solution while continuously agitating it for 15 min at 70℃. After the complete addition of the eucalyptus extract, the mixture was further agitated at 70℃ for 3 h, and pH was adjusted to 12, pH adjustment was achieved using a 1 M concentration solution of sulfuric acid and sodium hydroxide. The color of the mixture changes from dark yellow to light yellow. Demonstrates that ZnO NPs were created and that the reduction process took place. Vacuum filtration and numerous washes with distilled water and absolute ethanol were used to clear the yellow ZnO-NPs precipitate.

2.2. Characterization of ZnO NPs

Characterization of ZnO NPs was analyzed using a variety of characterization techniques to determine their structure, shape, size, and other key characteristics. SSA, pore size, and volume were determined using the (BET) analysis. Finally, (FT-IR) was applied to examine functional groups of ZnO NPs (Shimadzu, Japan).

2.3. Photoreactor

The photoreactor is designed to accomplish the photocatalysis process under UV-light radiation type A. 24 UV-A lamps (30 cm long, 2.2 cm broad, 8 W of power, 1 W/m^2 of light intensity, and a maximum wavelength peak of 365 nm) were put within a cylindrical aluminum container to create a reflecting surface for incident photons. The aluminum container is attached to a cube of wood with dimensions of (60 × 60 × 60 cm), and the spacing between the lights and the reaction room was reduced to ten centimeters. The photoreactor has two fans installed at the top that supply cooling air and protect the reaction vessel from the hot lamps; the temperature within the reactor is regulated between 30 and 40 C. The temperature inside the reaction cell and the light reactor was tracked using nine thermocouples evenly distributed throughout the device. The layout of the photoreactor is shown in Figure (1), and the buttons on the photoreactor indicate the number of lamps used in the system, for example, 6, 15, or 24 UV-A.

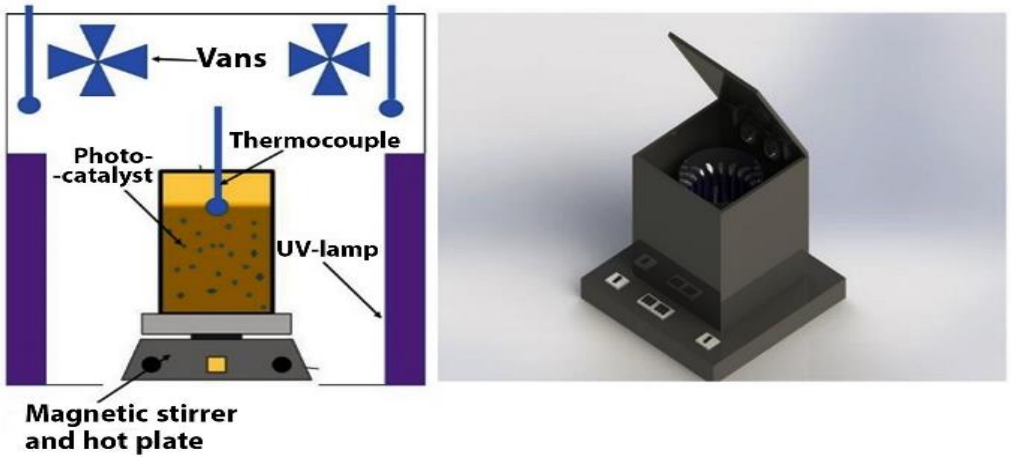

Figure (1): Schematic diagram of photo reactor.

2.4. Fixed Bed Design

A one-liter Pyrex beaker was used for photo-degradation tests of AB210 elimination by a photocatalytic technique. The effect of a number was examined during procedures, including pH levels between 2 and 9, temperature ranges between 25 and 55 °C, AB210 concentrations between 5 and 40 mg/L, and ZnO NPs levels between 0.1 and 1 g/L. First, the pH of the solutions was adjusted using 1 M sulfuric acid and 1 M sodium hydroxide. A photo reactor, depicted in Figure 1, was used to carry out the photocatalytic process. Throughout the experiment, samples were collected at regular intervals for 5,10,15,20,25,30,45,60,90,120, and 180 min and filtered using a 0.45 µm syringe filter. Lastly, the concentration of AB210 at a wavelength of 465 nm was measured using a UV/Vis.

The following equation was used to determine the removal effectiveness of AB210.

$$\%\mathbf{DR} = \frac{\mathbf{C_o - C_t}}{\mathbf{C_o}} \mathbf{x\ 100}\ \% \qquad \mathbf{(7)}$$

Where C_0 is the initial AB210, the final C_t is AB210 at the time, and % DR is the removal efficiency.

To accommodate the photo-reactor design, a column was particularly built. As a result, as illustrated in Figure (2), to control the flow, beads (1-1.5 mm) were placed 10 cm from bottom. Following the layer of glass beads, a specific amount of ZnO NPs was combined with beads and placed in the column. The remainder of the column was also covered with beads, making a 6 cm thick covering. Mesh 1 cm and 1 cm thick glass wool were used to stabilize the packed layers and prevent materials from moving down or up. The column must be filled with beads to create a uniform velocity profile. The dye solution was pumped upward using a peristaltic pump.

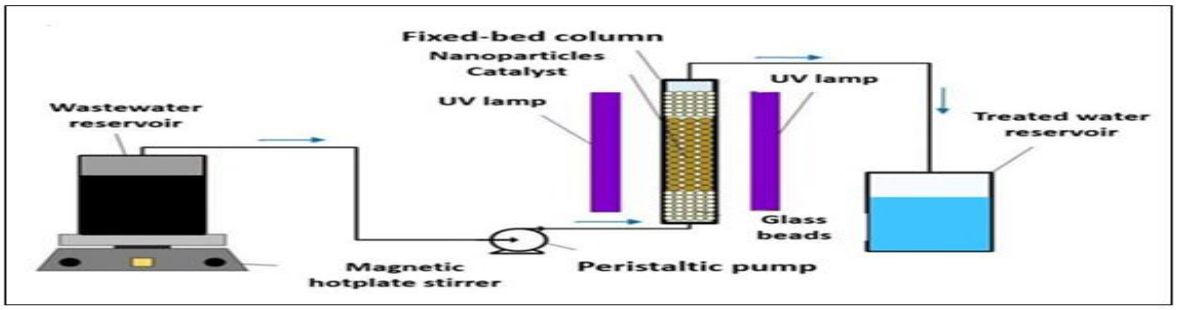

Figure (2): Continuous photocatalytic experiment for AB210 removal using fixed-bed column inside photoreactor (a) fixed-bed column, (b) photocatalytic system.

2.5. Design of Continuous Experiments

After the appropriate pH and temperature parameters were determined through batch experiments. Table (2) lists the various responses investigated throughout the fixed-bed operation. BBD was used to optimize the parameters under consideration.

The ratio of beads was varied together with the height of ZnO NPs during fixed-bed preparation to retain the overall height at 8 cm. Finally, the AB210 was injected into the column and passed through inert and NP-packed sections. Flow through the bed was continued until the AB210 (C_t) approached (0.9 C_o), at which point (t_e) was measured. Throughout the experiment, the solution was sampled and examined with a UV/VIS spectrophotometer.

Table (2): Coded symbols and ranges for continuous factors.

Factors	Levels in Box–Behnken design		
	Low (-1)	**Middle (0)**	**High (+1)**
A: Flow rate	1	3	5
B: ZnO-NPs (cm)	0.5	1	1.5
C: Dye Conc (mg/L)	5	22.5	40
D: UV-intensity	6	15	24

2.6. Analysis of Fixed Bed Data

(t_b) are essential characteristics for evaluating the fixed-bed design's dynamic reactivity and removal effectiveness. The breakthrough curve is produced by plotting the ratio of (C_t/C_0) against time. The exhaustion time (t_e) is the amount of time needed for the effluent dye concentration to approach the starting dye concentration by almost the same amount, while the time needed for the effluent dye concentration to reach 5% of the initial dye concentration is known as the (t_b). Additionally, when the dye's color does not change, indicating that the catalyst has reached saturation and the C_t/C_0 ratio of 0.9, the removal process is terminated. Furthermore, q_{total} was determined using the formula in equation (8):

$$\mathbf{q_{total} = \frac{QA}{1000} = \frac{QC_0}{1000}\int_{t_o}^{t_s} C_r\, dt} \qquad \mathbf{(8)}$$

Where A is the area under the curve C_r is the removal concentration (C_o- C_t) in (mg/L), and t_s is the saturation time (min), (m_{total}) the total quantity of dye that is fed to the fixed-bed column can be determined by the following equation (9):

$$\mathbf{m_{total} = \frac{C_0 Q\, x t_s}{1000}} \qquad \mathbf{(9)}$$

Additionally, the total removal efficiency (RE %) can be computed by the equation (10):

$$\mathbf{\%RE = \frac{q_{total}}{m_{total}}\ x\ 100} \qquad \mathbf{(10)}$$

Equation (11), was used to calculate (the EBCT) The term refers to the empty bed contact time is an important parameter of the relationship between the solute flows in the column with the packed or catalyst and can be expressed by the following equation:

$$\mathbf{EBCT} = \frac{\mathbf{V_C}}{\mathbf{Q}} \quad \textbf{(11)}$$

$$\mathbf{V_C} = \mathbf{A_C}\,\mathbf{Z} \quad \textbf{(12)}$$

Where V_C is the volume of the catalyst in the column (m^3) and A_c is the column cross-sectional area (m^2).

3. Results and Discussion

3.1. Characterizations of NPs

ZnO NPs functional groups were defined by Fourier-transformed Infrared Radiation (FT-IR) using a mid-IR (400-4000 cm^{-1}), as depicted in Figure (3). Significant eucalyptus leaf extract peaks exhibit bands at 3414 and 3425.5 cm^{-1} because of the O-H stretching of polyphenols [37, 38].

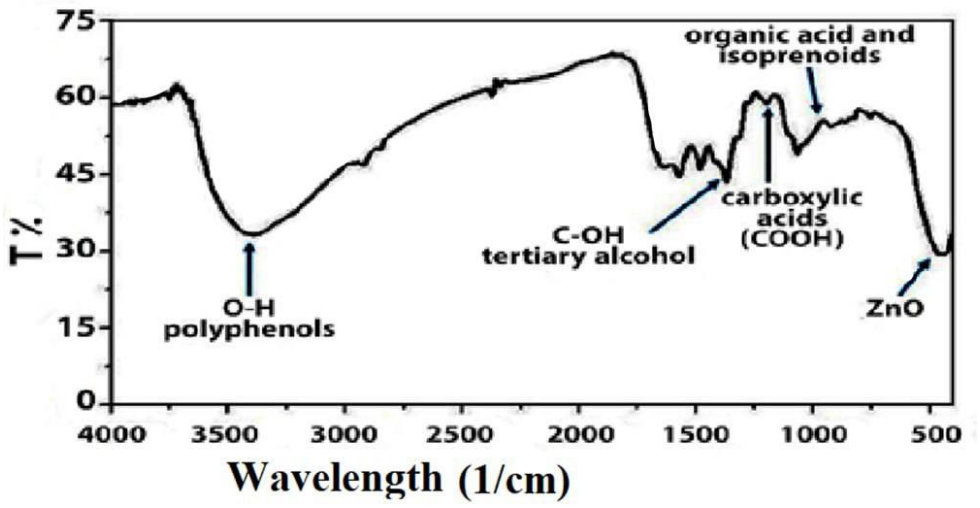

Figure (3): FT-IR of ZnO NPs.

The following band at 1543 cm^{-1} is associated with aromatic C═C stretching [39, 40]. Also, the band at 1481.3 cm^{-1} is caused by the presence of the tertiary alcohol (C-OH) group. Similarly, peaks have been observed at 869.9 cm^{-1} corresponding to the isoprenoids and organic acid in eucalyptus extract [23, 41]. These functional groups explain the presence of biomolecules in eucalyptus extract to prevent the aggregation of NPs. There are peaks between 439.7 and 416.6 cm^{-1} that indicate ZnO NPs [42, 43].

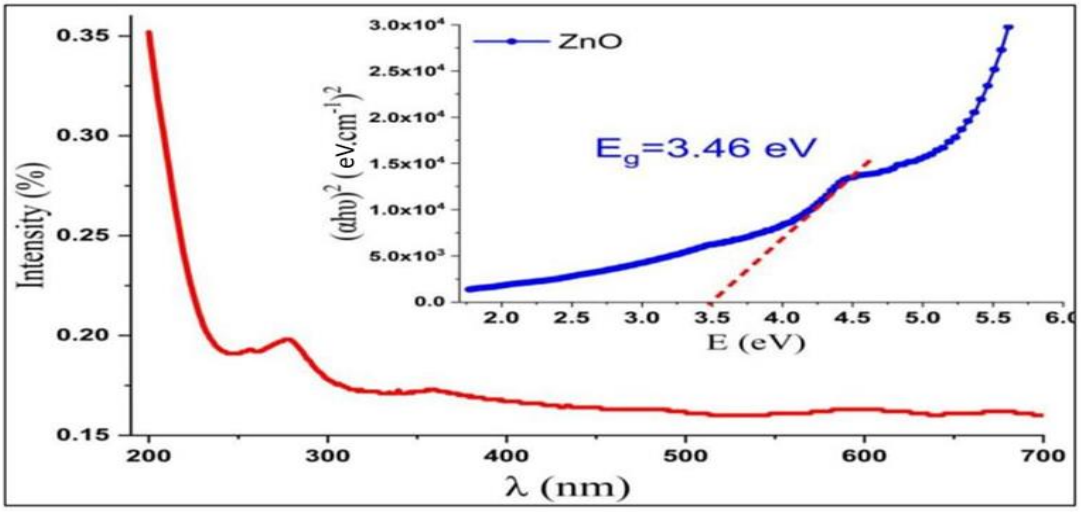

Figure (4): (a) UV-visible, (b) Band gap energy diagram of ZnO NPs.

The band gap energy of ZnO NPs was examined using a UV-Visible spectroscopy method analysis at wavelengths ranging from 200 to 700 nm, with the maximum peak at 358 nm and the band gap energy was calculated using the equation Eg = hc/λ, the maximum wavelength is 3.46 eV, as shown in Figure (4), which is consistent with recent results [44, 45]. The basic process of photocatalyst action is shown in Figure (5).

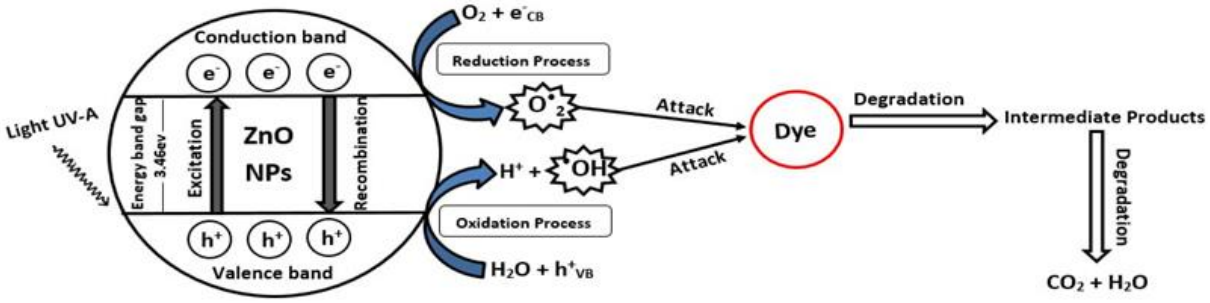

Figure (5): Basic principle of photocatalysis.

Photons (hv) higher than a (BG) must be absorbed. This causes electrons to flow from the valence band to the conduction band, forming a hole in the valence band. These divided holes and electrons can, nevertheless, these separated holes and electrons can rejoin and release the absorbed energy as heat. This photogenerated e- and h^+ then react with conveniently accessible oxidants and reductants to make potent and unstable radicals, which react with the contaminant and mineralize it to CO_2 and H_2O while forming a range of intermediary molecules [25, 46].

The scanning electron microscopy (SEM) analysis of ZnO nanoparticles (NPs) revealed their predominantly porous and spherical morphology, exhibiting a range of sizes spanning from 22 to 37 nm, as visually depicted in Figure (6). Moreover, the presence of polyphenol as a capping agent played a pivotal role in encapsulating the surface of ZnO NPs. This protective coating contributed to minimal agglomeration, thereby observed through SEM analysis [47, 48].

According to Figure (7), Zn, and O, are present in the sample, according to the NPs Energy Dispersive X-ray Spectroscopy EDAX analysis. The elevated intensities of the zinc and oxygen peaks indicate that ZnO constitutes the bulk of the sample. In the ZnO NPs sample, the weight percentages of zinc, and oxygen were 73.4%, and 4.619 %, respectively. Zinc's atomic percent was 59.32%, and oxygen's atomic percent was 29.26%. However, O indicated that polyphenols and other compounds were present in the eucalyptus leaf extract [47]. The application of a sample coating for SEM imaging resulted in the presence of gold. Furthermore, the analysis of the EDAX

spectrum revealed the existence of two distinct peaks corresponding to zinc at energy levels of one keV and eight keV, alongside a solitary peak representing O at a wavelength of 0.5 keV. These observations suggest Zinc is present as zinc oxide nanoparticles [12, 48].

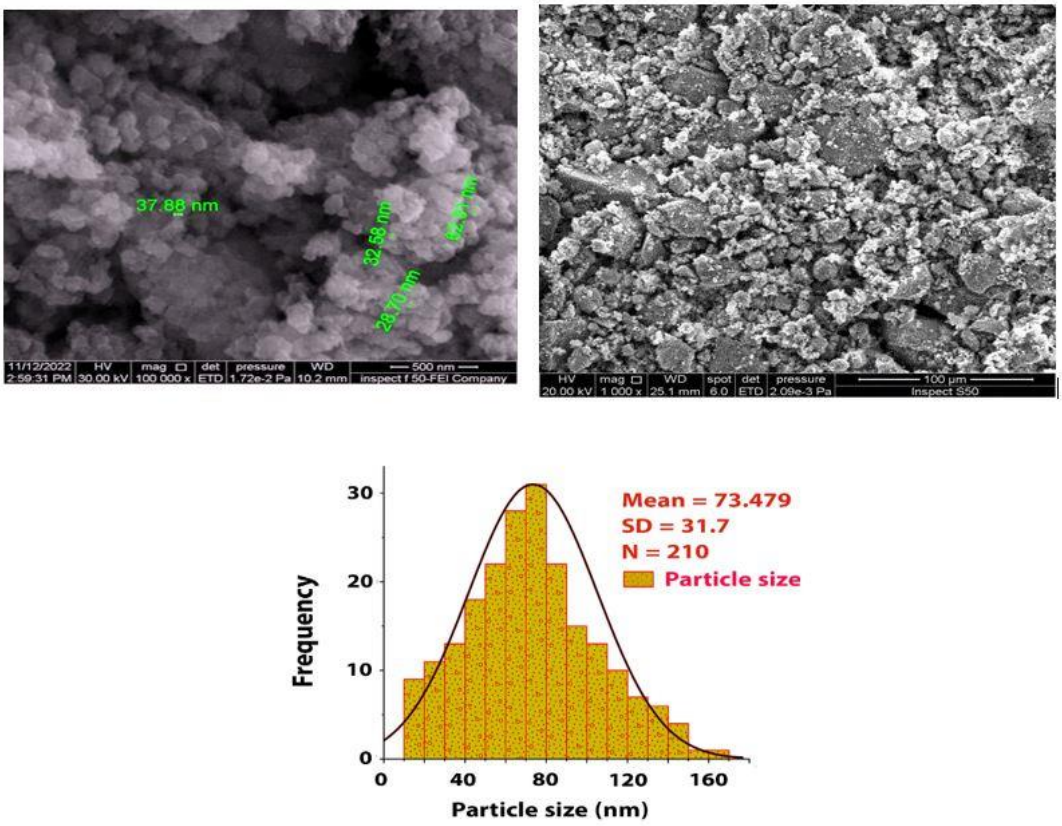

Figure (6): SEM image of ZnO NPs.

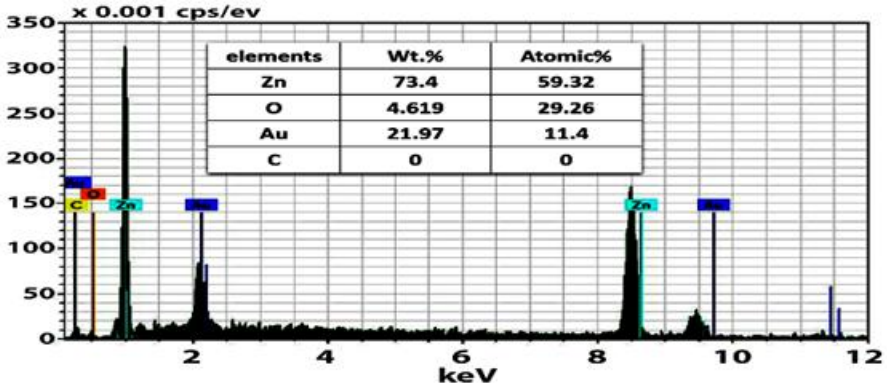

Figure (7): EDAX results of ZnO NPs.

ZnO NPs specific surface area (SSA), size, and pore volume were measured using Brunauer-Emmet-Teller (BET). Pore volume, SSA, and dimension were 26.318 m^2/g, 0.098 cm^3/g, and 11.118 nm, respectively. The findings suggest that ZnO NPs are mesoporous particles because the pore size is in the mesoporous particles [49, 50]. The high SSA illustrates the potential for affordable ZnO NPs to absorb pollutants [51].

Zeta potential determination is an important metric for analyzing particle stability. A high zeta potential indicates that nanoparticles are stable and resistant to aggregation. Conversely, a low zeta potential means that nanoparticles

are unstable and prone to flocculation. Figure (8) displays the zeta potential (ZP) study, which revealed a considerably negative value of -72.28 mV, suggesting the good stability of ZnO NPs [52]. This stability can be attributed to the presence of phenolic chemicals in the eucalyptus leaf extract [53].

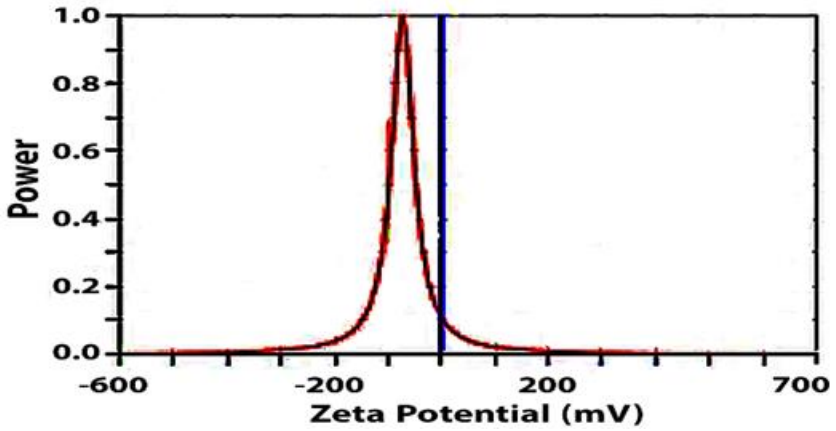

Figure (8): ZP of ZnO NPs.

Figure (9) illustrates 20 the characteristic peaks of ZnO NPs. at 31.59 °, 34.56°, 36.35°, 47.65°, 56.65°, 62.85°and 68.45°, for (010), (002), (011), (012), (110), (013), (021) planes of the crystal lattice, respectively [54], By comparing the results from (JCPDS), The spherical and hexagonal zinc oxide phases are responsible for all the diffraction peaks. The product possesses a well-crystalline particle structure, as seen by the diffraction peaks that are both narrow and robust [54].

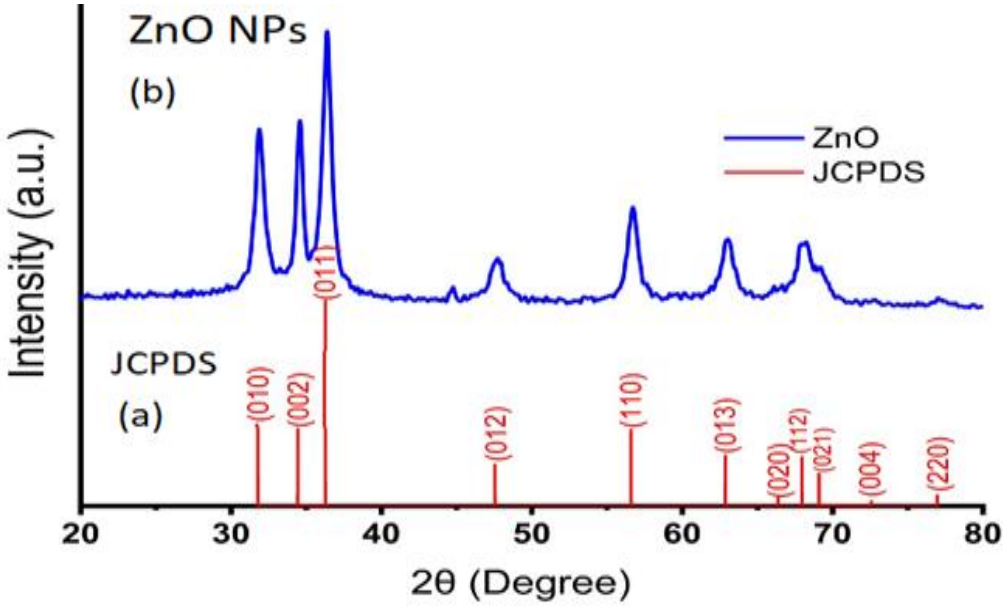

Figure (9): XRD of ZnO nanoparticles: (a) Standard XRD, and (b) ZnO NPs XRD.

Table (3): Results of the zinc oxide nanoparticle (ZnO NPs) characterization.

Technique	Parameter/Observation	Results	Reference
FT-IR	Functional groups and associated bands	Peaks at 3414 cm^{-1} and 3425.5 cm^{-1} (O-H stretching), 1543 cm^{-1} (aromatic C=C stretching), 1481.3 cm^{-1} (C-OH group), and 869.9 cm^{-1} (isoprenoids and organic acids). Peaks between 439.7 and 416.6 cm^{-1} indicate ZnO NPs.	[37, 43]
UV-Visible	Band gap energy	Absorption peak at 358 nm; band gap energy = 3.46 eV.	[44, 45]
SEM	Morphology and size	Porous and spherical morphology with particle sizes ranging from 22–37 nm.	[47, 48]
EDAX	Elemental composition	Zn (73.4 wt%, 59.32 %) and O (4.619 wt%, 29.26 %). Presence of gold due to coating for SEM imaging. Peaks at 1 keV, 8 keV (Zn), and 0.5 keV (O).	[12, 48]
BET	Specific surface area (SSA), pore volume, and pore size	SSA: 26.318 m^2/g; pore volume: 0.098 cm^3/g; pore size: 11.118 nm (mesoporous particles).	[49, 51]
Zeta Potential	Stability	-72.28 mV, indicating good stability of ZnO NPs.	[52, 53]
XRD	Crystallinity and phase	Peaks at 31.59°, 34.56°, 36.35°, 47.65°, 56.65°, 62.85°, and 68.45°, corresponding to hexagonal ZnO phase.	[54]

3.2. Statistical Methods for Continuous Data Analysis

The Supplementary material (Table S1) provides illustrations of the outcomes of ongoing photocatalytic investigations. With a regression coefficient R^2 of 0.99, the quadratic model Equation (13) showed the best fit to the experimental findings.

$$\%DR = = 69.58 - 8.12\,A + 3.96\,B + 2.67\,C + 0.6308\,D - 3.87\,AB - 8\,AC + 1.89\,AD + 1\,BC - 3\,CD - 8.02\,(A^2) - 2.01\,(B^2) + 2.55\,(c^2) - 1.36\,(D^2) \quad (13)$$

Figure (10) shows the significance of the suggested model by plotting the experimental versus predicted values, which represents a suitable tool for studying the significance of the suggested model. In addition, Table (4) also shows that the model F-value and P-value were 106.31 and < 0.0001, respectively, indicating the model is significant.

Table (4): ANOVA for model related to continuous photocatalytic for ZnO-NPs.

Sources	Sum of Squares	df	Mean Square	F-value	p-value	
Models	1861.51	14	132.96	106.31	< 0.0001	Significant
A-Flow rate	604.84	1	604.84	483.59	< 0.0001	
ZnO-NPs	156.6	1	125.21	125.21	< 0.0001	
C-Dye conc.	85.33	1	85.83	68.23	< 0.0001	
D-UV-intensity	4.23	1	4.23	3.38	0.0908	
AB	37.48	1	37.48	29.97	0.0001	
AC	256	1	256	204.68	< 0.0001	
A^2	299.77	1	299.77	239.68	< 0.0001	
B^2	21.19	1	21.19	16.94	0.0014	
C^2	36.86	1	36.86	29.47	0.0002	
D^2	9.21	1	9.21	7.37	0.0188	
Residual	15.01	12	1.25			
Lack of Fit	14.34	10	1.43	4.30	0.9792	not significant
Pure Error	0.6667	2	0.3333			
Cor Total	1876.52	26				
R^2	0.99					
Adjusted R^2 (R^2 adj)	0.9827					
Predicted R^2 (R^2 pre)	0.9524					
Adeq Precision	39.9893					
Std. Dev.	1.12					

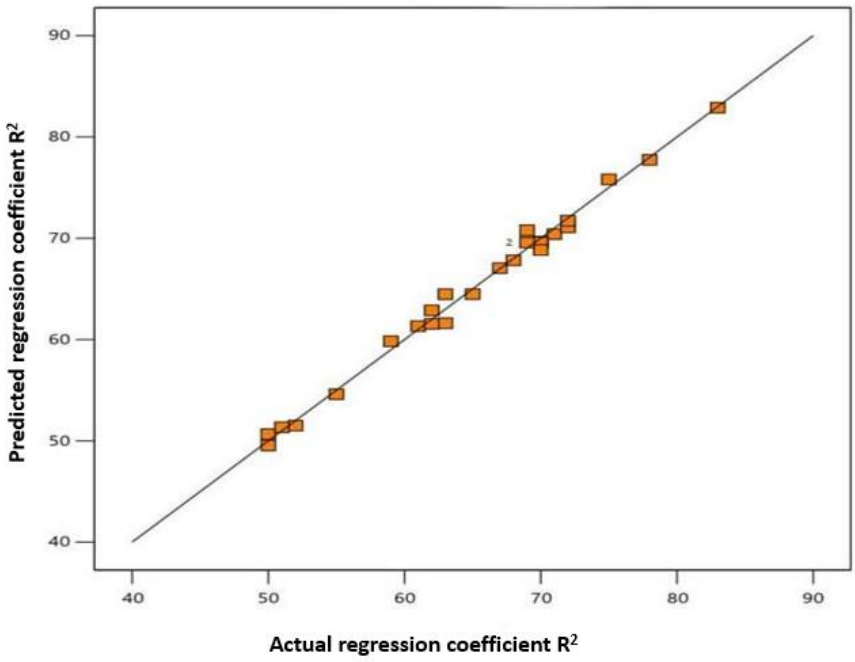

Figure (10): Predicted versus Actual responses of AB210 degradation through continuous Photocatalytic process (ZnO-NPs).

3.3. Effect of Parameters on AB210 Degradation through Continuous System

3.3.1. Interaction Effect of Flow Rate and Initial Dye Concentration

Figure (11) illustrates the interaction effect between flow rate and AB210 concentration. According to P-value and F-value estimated ANOVA analysis, the influent flow rate is most affected parameters on AB210 degradation efficiency. In addition, t_b time and t_e are highly dependent on the flow rate [55]. However, the uptake and removal efficiency for dye decreased with increased flow rate and its higher value at a lower flow rate. This phenomenon was possibly related to reducing the contact time between AB210 solution and catalyst at a higher flow rate, while it has more time to oxidized onto catalyst and complete the removal process with delay the exhaustion of the column. However, increases AB210 concentration led to decreases in the degradation efficiency of the column. Furthermore, when the concentration of AB210 reaches 40 mg/L. This phenomenon occurs as a result of dye molecules blocking the catalyst active site, inhibiting the catalytic process in the active site and preventing the creation of •OH. This explains why low initial AB210 concentrations have a longer breakthrough time and high degradation efficiency [56].

3.3.2. Interaction Effect of NPs and Flow Rate

Fixed-bed experiments were conducted at heights of 0.5, 1 and 1.5 cm to investigate the influence of ZnO-NPs height on AB210 deterioration. Figure (12) indicates that at a lower dye flow rate (1 mL/min), the degradation efficiency increases. The experimental data observed from breakthrough carve such as, exhaustion time (t_e), saturation time (t_s) and (q_{total}) are illustrated in the Supplementary material (Table S2).

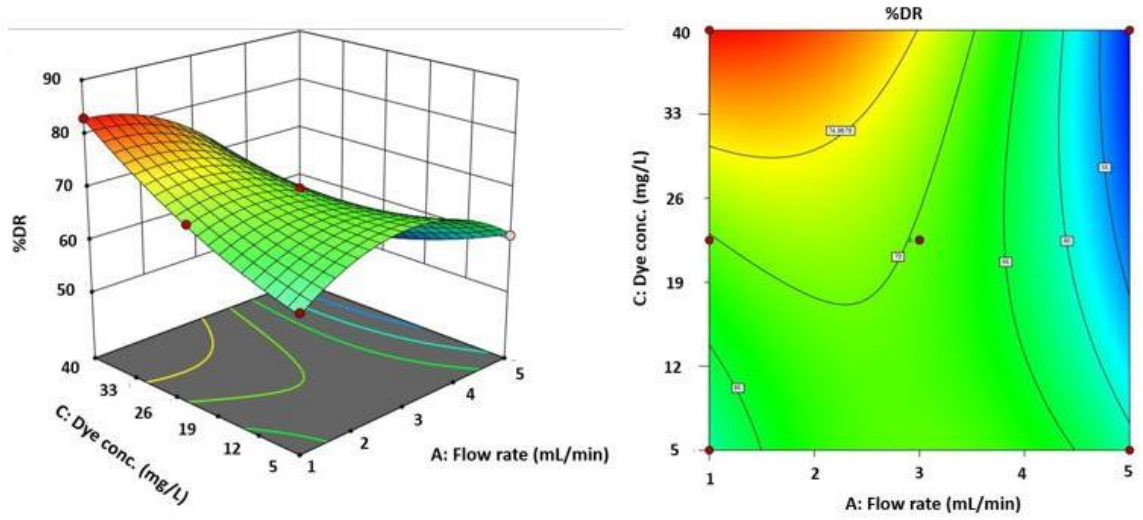

Figure (11): 3D surface and contour plot for interaction between flow rate and initial dye concentration in continuous photocatalytic process (ZnO-NPs).

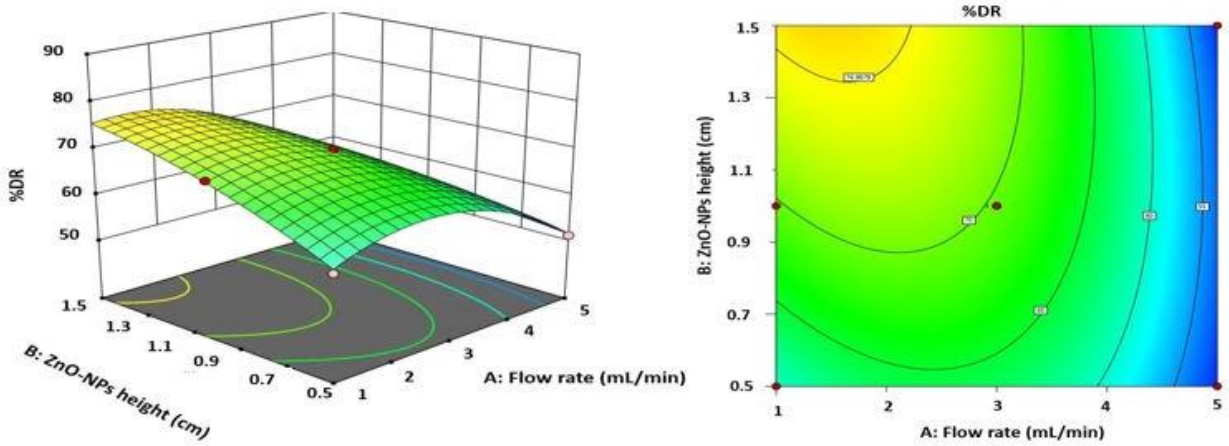

Figure (12): 3D surface and contour plot for interaction between flow rate and (ZnO-NPs) height in continuous photocatalytic process.

From this table, it is noted that, a flow rate of 1 ml/min, increasing the height of the ZnO-NPs induces an increase in the t_e and t_s because raising the height of the bed increases the contact time of the AB210 dye inside the fixed-bed column [57, 58].

3.3.3. Effect of UV-Intensity

Figure (13) illustrates how increasing UV intensity from (6-24 W/m^2) results in a higher degradation efficiency. Because it generated more photons, causing more electron-hole pairs to be excited and generating more •OH [59].

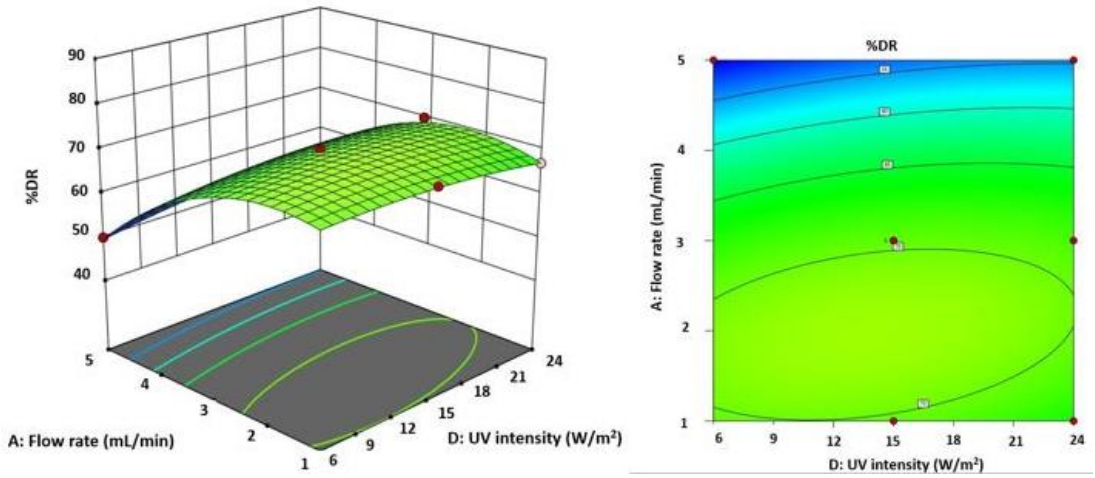

Figure (13): 3D surface and contour plot for interaction between flow rate and UV-intensity in continuous photocatalytic process (ZnO-NPs).

3.4. Fixed Bed Parameters Estimation

Several characteristics were extracted and shown using photocatalytic breakthrough curves (Table S2). Because the mass transfer rate was enhanced, increasing the flow rate resulted in a quicker (t_s). The amount of AB210 adsorbed onto ZnO-NPs (mass transfer zone) increased as a result [60]. Furthermore, the (t_e) was improved by decreasing the flow rate and increasing the ZnO-NPs height as the residence time of AB210 in the column increased [61]. The reason for increasing (t_b) by lowering the flow rate is that the pollutant has enough time to decay before exiting the column [62, 63]. Also see (Table S3) shown Minimum and maximum conditions for AB210 removal through continuous photocatalytic process (ZnO-NPs).

4. Conclusions

In conclusion, this study effectively demonstrated the efficacy of employing Eucalyptus plant extract for the environmentally friendly synthesis of Zinc oxide nanoparticles (ZnO NPs). A comprehensive array of analytical techniques, encompassing UV-Vis spectroscopy, FT-IR analysis, XRD, SEM, EDAX, BET, and Zeta potential, was utilized to assess the properties and quality of the bio-fabricated ZnO NPs. The characterization findings unveiled a porous nanoparticle architecture of the ZnO NPs, with an average dimension of 73.4 nm and a SSA of 26.318 m^2/g. The synthesized Zinc oxide nanoparticles (ZnO NPs) were utilized for the degradation of the photocatalytic process exhibited remarkable efficiency in comparison to adsorption, achieving a complete removal efficiency of 100%. The continuous photocatalytic process was carried out in a photoreactor using UV-A light. The quadratic model best fits the experimental responses in a continuous system, with the R^2 0.99 for the continuous photocatalytic experiment.

Acknowledgement: The authors are highly indebted to the Department of Biochemical Engineering, Al-Khwarizmi College of Engineering at the University of Baghdad and the Research and Technology Center of Environment, Water and Renewable Energy, Scientific Research Commission for providing facilities for the characterization of nanoparticles.

Conflict of Interest: The authors declare that there are no conflicts of interest associated with this research project. We have no financial or personal relationships that could potentially bias our work or influence the interpretation of the results.

References

[1] W. J. Fendi and J. A. Naser, "Adsorption Isotherms Study of Methylene Blue Dye on Membranes from Electrospun Nanofibers," *Orient. J. Chem.*, vol. 34, no. 6, pp. 2884–2894, 2018.

[2] A. N. Alene, G. Y. Abate, and A. T. Habte, "Bioadsorption of Basic Blue Dye from Aqueous Solution onto Raw and Modified Waste Ash as Economical Alternative Bioadsorbent," vol 23, no. 5,pp. 241–250, 2020.

[3] H. Agarwal, S. V. Kumar, and S. Rajeshkumar, "A review on green synthesis of zinc oxide nanoparticles – An eco-friendly approach," *Resour. Technol.*, vol. 3, no. 4, pp. 406–413, 2017.
[4] O. H. Fadhel, M. Y. Eisa, and Z. R. Zair, "Decolorizing of Malachite Green Dye by Adsorption Using Corn Leaves as Adsorbent Material," *J. Eng.*, vol. 27, no. 2, pp. 1–12, 2021.
[5] M. Jha, S. Ansari, and N. G. Shimpi, "Ultrasonic assisted green synthesis of Ag:CdO nanocubes and nanospheres using Citrus limon leaves for efficient degradation of organic dyes," *J. Ind. Eng. Chem.*, vol. 69, no. 5, pp. 269–284, 2019.
[6] H. B. W. Patterson, "Adsorption," *Bleach. Purifying Fats Oils Theory Pract.*, pp. 53–67, 2009.
[7] P. Taylor, S. S. Sonawane, S. Mishra, N. G. Shimpi, A. P. Rathod, and K. L. Wasewar, "Polymer-Plastics Technology and Engineering Comparative Study of the Mechanical and Thermal Properties of Polyamide-66 Filled with Commercial and Nano-Mg (OH)$_2$ Particles Comparative Study of the Mechanical and Thermal Properties of Polyamide-66 Filled with Commercial., vol. 49, no. 11, , pp. 37–41, 2014.
[8] Z. Monsef Khoshhesab and S. Souhani, "Adsorptive removal of reactive dyes from aqueous solutions using zinc oxide nanoparticles," *J. Chinese Chem. Soc.*, vol. 65, no. 12, pp. 1482–1490, 2018.
[9] M. Alkasir, N. Samadi, Z. Sabouri, Z. Mardani, M. Khatami, and M. Darroudi, "Evaluation cytotoxicity effects of biosynthesized zinc oxide nanoparticles using aqueous Linum Usitatissimum extract and investigation of their photocatalytic activityackn," *Inorg. Chem. Commun.*, vol. 119, no. 6, pp. 108066, 2020.
[10] T. H. Saleh, S. T. Hashim, S. N. Malik, and B. A. Laftaah Al-Rubaii, "Down-regulation of fliL gene expression by Ag nanoparticles and TiO_2 nanoparticles in pragmatic clinical isolates of Proteus mirabilis and Proteus vulgaris from urinary tract infection," *Nano Biomed. Eng.*, vol. 11, no. 4, pp. 321–332, 2019.
[11] B. I. Dheeb *et al.*, "Study the Antifungal Activity of ZnS:Mn Nanoparticles Against Some Isolated Pathogenic Fungi," *J. Phys. Conf. Ser.*, vol. 1178, no. 1, pp. 012008, 2019.
[12] A. A. Barzinjy and H. H. Azeez, "Green synthesis and characterization of zinc oxide nanoparticles using Eucalyptus globulus Labill . leaf extract and zinc nitrate hexahydrate salt," *SN Appl. Sci.*, vol. 2, no. 5, pp. 1–14, 2020.
[13] Kainat *et al.*, "Exploring the therapeutic potential of Hibiscus rosa sinensis synthesized cobalt oxide (Co3O4-NPs) and magnesium oxide nanoparticles (MgO-NPs)," *Saudi J. Biol. Sci.*, vol. 28, no. 9, pp. 5157–5167, 2021.
[14] K. A. Sukkar, A. A. Karamalluh, and T. N. Jaber, "Rheological and Thermal Properties of Lubricating Oil Enhanced by the Effect of CuO and TiO2 Nano-Additives," *Al-Khwarizmi Eng. J.*, vol. 15, no. 2, pp. 24–33, 2019.
[15] Z. Sabouri, S. Sabouri, S. S. Tabrizi Hafez Moghaddas, A. Mostafapour, M. S. Amiri, and M. Darroudi, "Facile green synthesis of Ag-doped ZnO/CaO nanocomposites with Caccinia macranthera seed extract and assessment of their cytotoxicity, antibacterial, and photocatalytic activity," *Bioprocess Biosyst. Eng.*, vol. 45, no. 11, pp. 1799–1809, 2022.
[16] A. K. Hassan, M. A. Atiya, and Z. A. Mahmoud, "Photo-Fenton-like degradation of direct blue 15 using fixed bed reactor containing bimetallic nanoparticles: Effects and Box–Behnken optimization," *Environ. Technol. Innov.*, vol. 28, no. 4, p. 102907, 2022.
[17] S. T. Bunyan and A. A.-K. M. Hasan, "Experimental Study of the Influence of Nanoparticles Additive to Diesel Fuel on the Emission Characteristics," *Al-Khwarizmi Eng. J.*, vol. 17, no. 1, pp. 13–19, 2021.
[18] T. Sen, S. Mishra, and N. G. Shimpi, "A b -cyclodextrin based binary dopant for polyaniline : Structural , thermal , electrical , and sensing performance," *Mater. Sci. Eng. B*, vol. 220, pp. 13–21, 2017.
[19] Y. A. Mustafa, A. I. Alwared, and M. Ebrahim, "Heterogeneous Photocatalytic Degradation for Treatment of Oil from Wastewater," *Al-Khwarizmi Eng. J.*, vol. 10, no. 3, pp. 53–61, 2014.
[20] S. J. Charde, S. S. Sonawane, A. P. Rathod, S. H. Sonawane, N. G. Shimpi, and V. R. Parate, "Copper-Doped Zinc Oxide Nanoparticles : Influence on Thermal , Thermo Mechanical , and Tribological Properties of Polycarbonate," pp. 1–9, 2017.
[21] A. M. Huerta-Flores, E. Luévano-Hipólito, L. M. Torres-Martínez, and A. Torres-Sánchez, "Photocatalytic H2 production and CO2 reduction on Cu, Ni-doped ZnO: effect of metal doping and oxygen vacancies," *J. Mater. Sci. Mater. Electron.*, vol. 30, no. 20, pp. 18506–18518, 2019.
[22] X. Liu, L. Ye, S. Liu, Y. Li, and X. Ji, "Photocatalytic reduction of CO2 by ZnO micro/nanomaterials with different morphologies and ratios of {0001} facets," *Sci. Rep.*, vol. 6, no. 12, pp. 1–9, 2016.
[23] M. Fazlzadeh, K. Rahmani, A. Zarei, H. Abdoallahzadeh, F. Nasiri, and R. Khosravi, "A novel green synthesis

of zero valent iron nanoparticles (NZVI) using three plant extracts and their efficient application for removal of Cr(VI) from aqueous solutions," *Adv. Powder Technol.*, vol. 28, no. 1, pp. 122–130, 2017.

[24] S. Chowdhury and R. Balasubramanian, "Graphene/semiconductor nanocomposites (GSNs) for heterogeneous photocatalytic decolorization of wastewaters contaminated with synthetic dyes: A review," *Appl. Catal. B Environ.*, vol. 160–161 no.6, pp. 307–324, 2014.

[25] L. V. Bora and R. K. Mewada, "Visible/solar light active photocatalysts for organic effluent treatment: Fundamentals, mechanisms and parametric review," *Renew. Sustain. Energy Rev.*, vol. 76, no. 10, pp. 1393–1421, 2017.

[26] A. Bouafia *et al.*, "Removal of hydrocarbons and heavy metals from petroleum water by modern green nanotechnology methods," *Sci. Rep.*, vol. 13, no. 1, p. 5637, 2023.

[27] V. A. Online, R. Yadav, and S. Mishra, "Synthesis and sensing applications of polyaniline nanocomposites: a review" , RSC Advances, vol. 6, no. 48, 2015, pp.42196–42222, 2016.

[28] M. Ahmad *et al.*, "Phytogenic fabrication of ZnO and gold decorated ZnO nanoparticles for photocatalytic degradation of Rhodamine B," *J. Environ. Chem. Eng.*, vol. 9, no. 1, pp. 104725, 2021.

[29] N. G. Shimpi, J. Verma, and S. Mishra, "Preparation, characterization and properties of poly(vinyl chloride)/$CaSO_4$ nanocomposites," *Polym. - Plast. Technol. Eng.*, vol. 48, no. 10, pp. 997–1001, 2009.

[30] Najm ZA, Atiya MA, and Hassan A K. Biogenesis Synthesis of ZnO NPs: Its adsorption and photocatalytic activity for removal of acid black 210 dye. Karbala International Journal of Modern Science, vol. 9, no. 3, pp.15, 2023.

[31] A. D. Mali, N. G. Shimpi, and S. Mishra, "Thermal, mechanical and morphological properties of surface-modified montmorillonite-reinforced Viton rubber nanocomposites," *Polym. Int.*, vol. 63, no. 2, pp. 338–346, 2014.

[32] Bonfante de Carvalho, C. et al. 'Degradation of Acid Black 210 by advanced oxidative processes: O_3 and O_3/UV', Ozone: Science and Engineering, vol. 40 no. 5, pp. 372–376, 2018.

[33] J. Santhoshkumar, S. V. Kumar, and S. Rajeshkumar, "Synthesis of zinc oxide nanoparticles using plant leaf extract against urinary tract infection pathogen," *Resour. Technol.*, vol. 3, no. 4, pp. 459–465, 2017.

[34] M. Khan, P. Ware, and N. Shimpi, "Synthesis of ZnO nanoparticles using peels of Passiflora foetida and study of its activity as an efficient catalyst for the degradation of hazardous organic dye," *SN Appl. Sci.*, vol. 3, no. 5, pp. 1–17, 2021.

[35] B. Gherbi *et al.*, "Effect of pH Value on the Bandgap Energy and Particles Size for Biosynthesis of ZnO Nanoparticles: Efficiency for Photocatalytic Adsorption of Methyl Orange," *Sustain.*, vol. 14, no. 18, pp.11300, 2022.

[36] S. S. Ahmed *et al.*, "Green Synthesis, Characterizations of Zinc Oxide Nanoparticles from Aqueous Leaf Extract of Tridax procumbens Linn. and Assessment of their Anti-Hyperglycemic Activity in Streptozoticin-Induced Diabetic Rats," *Materials (Basel).*, vol. 15, no. 22, pp. 8202, 2022.

[37] S. Khanam and S. K. Rout, "A Photocatalytic Hydrolysis and Degradation of Toxic Dyes by Using Plasmonic Metal–Semiconductor Heterostructures: A Review," *Chem.*, vol. 4, no. 2, pp. 454–479, 2022.

[38] S. Vasantharaj *et al.*, "Enhanced photocatalytic degradation of water pollutants using bio-green synthesis of zinc oxide nanoparticles (ZnO NPs)," *J. Environ. Chem. Eng.*, vol. 9, no. 4, p. 105772, 2021.

[39] X. Weng, Z. Chen, Z. Chen, M. Megharaj, and R. Naidu, "Clay supported bimetallic Fe/Ni nanoparticles used for reductive degradation of amoxicillin in aqueous solution: Characterization and kinetics," *Colloids Surfaces A Physicochem. Eng. Asp.*, vol. 443, no. 3, pp. 404–409, 2014.

[40] M. S. Khan, P. P. Dhavan, B. L. Jadhav, and N. G. Shimpi, "Ultrasound-Assisted Green Synthesis of Ag-Decorated ZnO Nanoparticles UsingExcoecaria agallochaLeaf Extract and Evaluation of Their Photocatalytic and Biological Activity, vol. 5, no. 41, pp. 12660–12671, 2020.

[41] A. P. Shah, S. Jain, and N. G. Shimpi, "Enhanced Photocatalytic Activity of Electrospun PAN/Ag-G NFs Under Solar Irradiation for Effective Degradation of Hazardous Organic Dyes," *ChemistrySelect*, vol. 5, no. 13, pp. 3897–3905, 2020.

[42] K. Sravanthi, D. Ayodhya, and P. Y. Swamy, "Green synthesis, characterization and catalytic activity of 4-nitrophenol reduction and formation of benzimidazoles using bentonite supported zero valent iron nanoparticles," *Mater. Sci. Energy Technol.*, vol. 2, no. 2, pp. 298–307, 2019.

[43] A. P. Shah, A. S. Sharma, V. S. Sharma, and N. Shimpi, Polyacrylonitrile Nanofibers Incorporating Ag-Decorated Graphitic Carbon Nitride for the Visible-Light-Activated Selective Oxidation of Styrene , Benzylic

Methylene Groups , and Benzene Polyacrylonitrile Nanofibers Incorporating Ag-Decorated Graphitic Carbon Nitride for the Visible-Light-Activated Selective Oxidation of Styrene , Benzylic Methylene Groups , and Benzene, vol. 12, no. 12, pp. 3049, 2019.

[44] R. Ullah *et al.*, "In vitro and in vivo applications of Euphorbia wallichii shoot extract-mediated gold nanospheres," *Green Process. Synth.*, vol. 10, no. 1, pp. 101–111, 2021.

[45] S. Jain, N. Karmakar, A. Shah, and N. G. Shimpi, "Development of Ni doped ZnO/polyaniline nanocomposites as high response room temperature NO2 sensor," *Mater. Sci. Eng. B Solid-State Mater. Adv. Technol.*, vol. 247, no. 5, p. 114381, 2019.

[46] V. A., "Synthesis and sensing applications of polyaniline nanocomposites: a review", RSC Advances, vol. 6, no. 48, 2015, pp.42196–42222, 2016.

[47] M. Imran *et al.*, "In vitro examination of anti-parasitic, anti-Alzheimer, insecticidal and cytotoxic potential of Ajuga bracteosa Wallich leaves extracts," *Saudi J. Biol. Sci.*, vol. 28, no. 5, pp. 3031–3036, 2021.

[48] T. Sen, N. G. Shimpi, S. Mishra, and R. Sharma, Simultaneous electrochemical determination of epinephrine and uric acid in the presence of ascorbic acid using SnO_2/graphene nanocomposite modified glassy carbon electrode, Sensors Actuators *B.* Chem., vol. 221, no. 3, pp. 1412–1422, 2015.

[49] S. Pai, S. H, T. Varadavenkatesan, R. Vinayagam, and R. Selvaraj, "Photocatalytic zinc oxide nanoparticles synthesis using Peltophorum pterocarpum leaf extract and their characterization," *Optik (Stuttg).*, vol. 185, no. 2, pp. 248–255, 2019.

[50] S. Mishra and N. G. Shimpi, "Mechanical and Flame-Retarding Properties of Styrene – Butadiene Rubber Filled with Nano-$CaCO_3$ as a Filler and Linseed Oil as an Extender," vol. 5, no.9, pp. 134 –150, 2005.

[51] A. T. Mansour *et al.*, "Green Synthesis of Zinc Oxide Nanoparticles Using Red Seaweed for the Elimination of Organic Toxic Dye from an Aqueous Solution," *Materials (Basel).*, vol. 15, no. 15, pp. 1–25, 2022.

[52] J. Khan *et al.*, "Kinetic and thermodynamic study of oxidative degradation of acid yellow 17 dye by Fenton-like process: Effect of HCO_3^-, CO_3^{2-}, Cl^- and SO_4^{2-} on dye degradation," *Bull. Chem. Soc. Ethiop.*, vol. 33, no. 2, pp. 243–254, 2019.

[53] A. R. Puthukkara P, S. Jose T, and D. lal S, "Plant mediated synthesis of zero valent iron nanoparticles and its application in water treatment," *J. Environ. Chem. Eng.*, vol. 9, no. 1, p. 104569, 2021.

[54] R. P. Singh, V. K. Shukla, R. S. Yadav, P. K. Sharma, P. K. Singh, and A. C. Pandey, "Biological approach of zinc oxide nanoparticles formation and its characterization," *Adv. Mater. Lett.*, vol. 2, no. 4, pp. 313–317, 2011.

[55] A. S. Mahmoud, A. Ismail, M. K. Mostafa, M. S. Mahmoud, W. Ali, and A. M. Shawky, "Isotherm and kinetic studies for heptachlor removal from aqueous solution using Fe/Cu nanoparticles, artificial intelligence, and regression analysis," *Sep. Sci. Technol.*, vol. 55, no. 4, pp. 684–696, 2020.

[56] L. Chen *et al.*, "Preparation of TiO2 nanofilm via sol-gel process and its photocatalytic activity for degradation of methyl orange," *Ceram. Int.*, vol. 35, no. 8, pp. 3275–3280, 2009.

[57] S. Mishra, N. G. Shimpi, and U. D. Patil, "Effect of Nano $CaCO_3$ on thermal properties of Styrene Butadiene Rubber (SBR)," vol.8, no.7,pp. 449–459, 2007.

[58] S. Azizi, M. M. Shahri, and R. Mohamad, "Green synthesis of zinc oxide nanoparticles for enhanced adsorption of lead Ions from aqueous solutions: Equilibrium, kinetic and thermodynamic studies," *Molecules*, vol. 22, no. 6, pp. 831, 2017.

[59] G. E. Lau *et al.*, "Eco-Friendly Photocatalysts for Degradation of Dyes", *Catalyts*, vol. 10, no. 10, pp. 1129, 2020.

[60] V. C., M. N. C. Prabha, and M. A. L. A. Raj, "Green mediated synthesis of zinc oxide nanoparticles for the photocatalytic degradation of Rose Bengal dye," *Environ. Nanotechnology, Monit. Manag.*, vol. 6, no.2, pp. 134–138, 2016.

[61] M. N. Zafar, Q. Dar, F. Nawaz, M. N. Zafar, M. Iqbal, and M. F. Nazar, "Effective adsorptive removal of azo dyes over spherical ZnO nanoparticles," *J. Mater. Res. Technol*, vol. 8, no. 1, pp. 449–459, 2018.

[62] B. Uzair *et al.*, "Green and cost-effective synthesis of metallic nanoparticles by algae: Safe methods for translational medicine," *Bioengineering*, vol. 7, no. 4, pp. 1–22, 2020.

[63] U. Wijesinghe, G. Thiripuranathar, H. Iqbal, and F. Menaa, "Biomimetic synthesis, characterization, and evaluation of fluorescence resonance energy transfer, photoluminescence, and photocatalytic activity of zinc oxide nanoparticles," *Sustain.*, vol. 13, no. 4, pp. 1–22, 2021.

Supplementary Materials

Table (S1): The actual and predicted responses of continuous photocatalytic experiments for ZnO-NPs.

Exp.	A: Flow rate (ml/min)	B: ZnO-NPs Hight (cm)	C: AB210 concentration (mg/L)	D: UV-intensity (W/m^2)	Actual responses %	Predicted responses %
1	5	1	40	15	50	50.66
2	3	1	5	6	63	64.48
3	3	0.5	22.5	24	62	62.88
4	5	1	5	15	61	61.32
5	3	1.5	5	15	71	70.41
6	3	0.5	5	15	65	64.49
7	5	0.5	22.5	15	51	51.34
8	5	1.5	22.5	15	52	51.51
9	3	0.5	22.5	6	63	61.62
10	3	1	5	24	72	71.74
11	3	1.5	22.5	24	69	70.8
12	1	1	40	15	83	82.89
13	5	1	22.5	24	55	54.61
14	3	0.5	40	15	68	67.83
15	3	1.5	22.5	6	70	69.54
16	3	1	40	24	72	71.07
17	3	1	22.5	15	70	69.58
18	3	1.5	40	15	78	77.74
19	3	1.5	22.5	24	70	68.85
20	1	1	22.5	24	67	67.05
21	3	1	40	6	75	75.81
22	1	0.5	22.5	15	59	59.83
23	1	1	5	15	62	61.56
24	3	1	22.5	15	69	69.58
25	3	1	22.5	15	69	69.58
26	5	1	22.5	6	50	49.56
27	1	1	22.5	15	70	69.67

Table (S2): The breakthrough experimental parameters of fixed-bed column (ZnO-NPs).

EXP	Q (ml/min)	Co (mg/L)	Z (cm)	*tb*(min)	*te*(min)	*ts*(min)	*Veff* (ml)	*Qtotal* (mg)	Mtotal	*RE* (%)	Vc (cm^3)	*LMTZ* (cm)	*EBCT* (min)	*qb* (mg/g)	*Vb* ml	*Uf* (cm/min	*tr* (min)
1	5	40	1	22	65	45	325	12.34	17.82	57	3.7	0.62	0.75	3.17	225	2.63	0.76
2	3	5	1	30	200	140	600	4.43	6.32	70	3.7	0.85	1.26	0.5	90	1.18	1.26
3	3	22.5	0.5	30	220	155	660	13.79	6.32	66	1.89	0.43	0.63	2.96	90	1.21	0.63
4	5	5	1	15	190	125	950	5.31	8.07	66	3.7	0.92	0.75	0.33	75	2.62	0.76
5	3	5	1.5	10	230	175	690	7.15	9.39	76	5.6	1.43	1.89	0.13	30	1.18	1.9
6	3	5	0.5	10	260	185	780	5.85	8.22	71	1.89	0.48	0.63	0.35	30	1.58	0.63
7	5	22.5	0.5	20	150	85	750	13.09	23.11	57	1.89	0.43	0.37	3.42	100	2.60	0.38
8	5	22.5	1.5	42	180	112	900	18.10	29.09	59	5.6	1.15	1.13	2.26	210	2.60	1.14
9	3	22.5	0.5	43	270	184	840	24.9	36.57	66	1.89	0.45	0.63	2.41	75	1.21	0.63
10	3	5	1	10	210	155	630	4.65	6.30	74	3.79	0.95	1.26	0.15	30	1.2	1.26
11	3	22.5	1.5	25	280	190	600	16.51	24.34	75	3.7	0.85	1.26	1.38	90	1.2	1.26
12	1	40	1	90	230	200	230	8.00	9.20	85	3.7	0.61	3.79	1.89	90	3.91	3.79
13	5	22.5	1.5	15	120	72	600	8.95	14.93	60	3.8	0.87	0.75	0.98	75	2.60	0.76
14	3	40	0.5	30	180	140	540	20.77	26.70	75	1.89	0.41	0.63	4.9	90	1.18	0.63
15	3	22.5	1.5	30	220	160	660	14.23	19.57	73	3.7	0.86	1.26	1.40	90	1.20	1.26
16	3	40	1	22	160	120	480	17.08	22.78	75	3.7	0.86	1.26	1.64	66	1.20	1.26
17	3	22.5	1	41	266	190	798	28.6	39.15	73	3.8	0.84	1.27	3.41	132	1.18	1.27
18	3	40	1.5	35	180	150	540	19.49	23.89	83	5.6	1.20	1.89	1.51	105	1.20	1.9
19	3	22.5	1	40	250	180	750	38	53.19	72	1.9	0.43	0.63	7.02	90	1.18	0.63
20	1	22.5	1	90	210	140	210	3.61	5.42	72	3.7	0.57	3.79	1.22	90	0.39	3.79
21	3	40	1	35	180	140	540	18.76	24.12	78	3.7	0.80	1.26	2.46	105	1.20	1.26
22	1	22.5	0.5	90	200	122	200	3.11	5.11	61	1.9	0.27	1.9	2.55	90	0.39	1.9
23	1	5	1	30	197	108	197	24.5	44.68	65	3.8	0.78	0.76	2.11	230	2.63	0.76
24	3	22.5	1	30	195	112	585	25.4	44.23	73	3.8	0.78	0.76	5.25	2.63	2.63	0.76
25	3	22.5	1	53	170	120	510	9.32	13.21	72	3.7	0.68	1.26	2.16	1.18	1.18	1.26
26	5	22.5	1	42	294	169	147	27.4	48.08	55	3.7	0.86	0.75	1.31	2.63	2.63	0.76
27	1	22.5	1.5	85	250	190	250	4.98	6.56	37	5.6	0.99	5.69	0.74	3.90	3.90	5.69

Table (S3): Minimum and maximum conditions for AB210 removal through continuous photocatalytic process (ZnO-NPs).

Parameters	Minimum removal	Maximum removal
A: Flow rate (mL/min)	5	2.25
B: ZnO-NPs hight (cm)	1	1.21
C: Dye conc. (mg/L)	40	30
D: UV-intensity (W/m^2)	15	15
DR %	57	69